

3. 研究成果の刊行に関する一覧・別刷

研究成果の刊行に関する一覧表
【H23. 4. 1～H24. 3. 31】

雑誌

発表者氏名	論文タイトル名	発表誌名	巻号	ページ	出版年
S. Yamaguchi, T. Kizuki, H. Takadama, T. Matsushita, T. Nakamura, T. Kokubo	Formation of a bioactive calcium titanate layer on gum metal by chemical treatment	J Mater Sci: Mater Med	23(4)	873-83	2012
D.K. Pattanayak, S. Yamaguchi, T. Matsushita, T. Nakamura, T. Kokubo	Apatite-forming ability of titanium in terms of pH of the exposed solution,	J Royal Society:Interface,	On line	Mar. 14	2012
D.K. Pattanayak, A. Fukuda, T. Matsushita, M. Takemoto, S. Fujibayashi, K. Sasaki, N. Nishida, T. Nakamura, T. Kokubo,	Bioactive Ti metal analogous to human cancellous bone: Fabrication by selective laser melting and chemical treatments.	Acta Biomater	7(3)	1398-406	2011
S. Fujibayashi, M. Takemoto, M. Neo, T. Matsushita, T. Kokubo, K. Doi, T. Ito, A. Shimizu, T. Nakamura,	A novel synthetic material for spinal fusion: a prospective clinical trial of porous bioactive titanium metal for lumbar interbody fusion.	Eur Spine J	20(9)	1486-95	2011
A. Fukuda, M. Takemoto, T. Saito, S. Fujibayashi, M. Neo, D.K. Pattanayak, T. Matsushita, K. Sasaki, N. Nishida, T. Kokubo, T. Nakamura,	Osteoinduction of porous Ti implants with a channel structure fabricated by selective laser melting	Acta Biomaterialia	7(5)	2327- 2336	2011

発表者氏名	論文タイトル名	発表誌名	巻号	ページ	出版年
A. Fukuda, M. Takemoto, T. Saito, S. Fujibayashi, M. Neo, S. Yamaguchi, T. Kizuki, T. Matsushita, M. Niinomi, T. Kokubo, T. Nakamura,	Bone-bonding bioactivity of Ti metal and Ti-Zr-Nb-Ta alloys with Ca ions incorporated on their surfaces by simple chemical and heat treatments.	Acta Biomater	7(3)	1379-86	2011
S. Yamaguchi, H. Takadama, T. Matsushita, T. Nakamura, T. Kokubo	Preparation of bio-active Ti-15Zr-4Nb-4Ta alloy from HCl and heat treatments after an NaOH treatment	J Biomed Mater Res Part A	97A(2)	135- 144	2011
H. Oonishi, H. Akiyama, M. Takemoto, T. Kawai, K. Yamamoto, T. Yamamuro, H. Oonishi, T. Nakamura,	The long-term in vivo behavior of polymethyl methacrylate bone cement in total hip arthroplasty.	Acta Orhop	82(5)	553-8	2011
H. Akiyama, T. Morishima, M. Takemoto, K. Yamamoto, H. Otsuka, T. Iwase, T. Kabata, T. Soeda, K. Kawanabe, K. Sato, T. Nakamura,	A novel technique for impaction bone grafting in acetabular reconstruction of revision total hip arthroplasty using an ex vivo compaction device.	J Orthop Sci	16(1)	26-37	2011
D.K. Pattanayak, S. Yamaguchi, T. Matsushita, T. Kokubo	Nano-structured positively charged bioactive TiO ₂ layer formed on Ti metal by NaOH, acid and heat treatments	J Mater Sci: Mater Med	22	1803- 1812	2011

Formation of a bioactive calcium titanate layer on gum metal by chemical treatment

Seiji Yamaguchi · Takashi Kizuki · Hiroaki Takadama ·
Tomiharu Matsushita · Takashi Nakamura ·
Tadashi Kokubo

Received: 5 October 2011 / Accepted: 27 January 2012 / Published online: 16 February 2012
© Springer Science+Business Media, LLC 2012

Abstract The so-called gum metal with the composition Ti–36Nb–2Ta–3Zr–0.3O is free from cytotoxic elements and exhibits a low elastic modulus as well as high mechanical strength. In the present study, it was shown that this alloy exhibited a high capacity for apatite formation in a simulated body fluid when subjected to 1 M NaOH treatment, 100 mM CaCl₂ treatment, heat treatment at 700°C, and then hot water treatment. The high apatite formation was attributed to the CaTi₂O₅ which was precipitated on its surface, and found to be maintained even in a humid environment over a long period. The treated surface exhibited high scratch resistance, which is likely to be useful in clinical applications. The surface treatment had little effect on the unique mechanical properties described above. These results show that gum metal subjected to the

present surface treatments exhibits a high potential for bone-bonding, which will be useful in orthopedic and dental implants.

1 Introduction

Various kinds of chemical and heat treatments have been proposed to induce bone-bonding bioactive characteristics in Ti metals [1–8]. Among them, treatment with NaOH and heat is the simplest and most commonly used. This treatment is already applied to artificial hip joints, and has been clinically used in Japan since 2007 [9]. This treatment is also effective in inducing bioactivity in conventional titanium alloys such as Ti–6Al–4V and Ti–15Mo–5Zr–3Al [10, 11]. However, it is not effective for certain new kinds of Ti–Zr–Nb–Ta alloys [12], which are free of elements suspected of cytotoxicity [13], such as vanadium. For Ti–15Zr–4Nb–4Ta alloy [14], one of the Ti–Zr–Nb–Ta alloys, it was shown that HCl and heat treatment [15], or CaCl₂, heat and water [16, 17] after the NaOH treatment, are effective for inducing bioactivity. However, even these treatments are not effective for the gum metal with the composition Ti–36Nb–2Ta–3Zr–0.3O [18], which has certain favorable mechanical properties such as a low elastic modulus and high mechanical strength, as well as a capacity for extensive elastic deformation and clayey plasticity, which are attractive features for use in orthopedic and dental implants.

In the present study, the gum metals were subjected to various kinds of chemical and heat treatments. Apatite formation in the treated gum metals was examined in a simulated body fluid (SBF). Their apatite-forming capacity was discussed in terms of their surface structural changes due to the treatments. It has been revealed for Ti metal and

S. Yamaguchi: Research Fellow of the Japan Society for the Promotion of Science.

S. Yamaguchi (✉) · T. Kizuki · H. Takadama · T. Matsushita ·
T. Kokubo
Department of Biomedical Sciences, Chubu University,
1200 Matsumoto-cho, Kasugai, Aichi 487-8501, Japan
e-mail: sy-esi@isc.chubu.ac.jp

T. Kizuki
e-mail: t-kizuki@isc.chubu.ac.jp

H. Takadama
e-mail: takadama@isc.chubu.ac.jp

T. Matsushita
e-mail: matsushi@isc.chubu.ac.jp

T. Kokubo
e-mail: Kokubo@isc.chubu.ac.jp

T. Nakamura
Kyoto Medical Center, National Hospital Organization, 1-1,
Fukakusa Mukaihata-cho, Fushimi-ku, Kyoto 612-8555, Japan
e-mail: ntakantaka@nifty.com

various kinds of Ti alloys that metals able to form bone-like apatite on their surfaces in SBF bond to living bone through the apatite layer formed on their surface in the living body [10, 11, 16, 19–23].

2 Materials and methods

2.1 Chemical and heat treatments

The Ti–36Nb–2Ta–3Zr–0.3O alloy sheet (Toyota Central Research and Development Laboratories, Inc., Ti: Bal., Nb: 36.39, Ta: 2.00, Zr: 2.87, O: 0.31, Fe: 0.02 mass%) was cut into rectangular plates which were $10 \times 10 \times 1 \text{ mm}^3$ in size, abraded with #400 diamond plates, and washed with acetone, 2-propanol and ultrapure water in an ultrasonic cleaner for 30 min each and dried at 40°C. These samples were soaked in 5 ml of a 1, 2 or 5 M NaOH aqueous solution at 60°C for 24 h. After removal from the solution, they were gently rinsed with ultrapure water for 30 s and dried at 40°C. (This treatment is designated “XM NaOH”, where X is 1, 2, or 5, depending on the NaOH concentrations.) The treated samples were subsequently soaked in 10 ml of 100 mM CaCl₂ solution at 40°C for 24 h, and washed with ultrapure water and dried. (This treatment is designated “CaCl₂”.) They were heated up to 600, 700, 800, or 900°C at a rate of 5°C min⁻¹, kept for 1 h at the respective temperature in an ambient atmosphere, and then this was followed by natural cooling in an electrical furnace. (This treatment is designated “heatY”, where Y is 600, 700, 800, or 900, depending on their heating temperatures.) After the heat treatment, they were soaked in 10 ml of ultrapure water at 80°C for 24 h, then washed and dried. (This treatment is designated “water”; thus, the sequence of the treatments is designated “XM NaOH–CaCl₂–heatY–water”, where X is 1, 2, or 5, and Y is 600, 700, 800, or 900.)

2.2 Surface analyses

The sample surfaces which were subjected to the chemical and heat treatments were analyzed by means of a field emission scanning electron microscope (FE-SEM: S-4300, Hitachi Co., Tokyo, Japan) equipped with an energy dispersive X-ray spectrometer (EDX: EMAX-7000, Horiba Ltd., Kyoto, Japan), an Auger electron spectrometer (AES: PHI-670, Ulvac-PHI Ink., Kanagawa, Japan), a thin-film X-ray diffractometer (TF-XRD: RINT-2500, Rigaku Co., Tokyo, Japan) and a Fourier transform confocal laser Raman spectrometer (FT-Raman: LabRAM HR800, Horiba Jovin Yvon, France). In the FE-SEM, the surface was coated with a Pt–Pd thin film, and a voltage of 15 kV was used, whereas in the EDX, an uncoated surface was analyzed at 5 kV–K for Ca and O, 5 kV–L for Ti, Zr and Nb,

and 5 kV–M for Ta on five areas, and their averaged value was used in our analysis. In AES measurement, the surface area of $40 \times 40 \mu\text{m}^2$ was analyzed at a take-off angle of 30° using electron beam of 5 kV and beam current of 50 nA with Ar⁺ sputtering at a rate of 12 nm min⁻¹ (SiO₂ conversion). In the TF-XRD measurement, a Cu-K α X-ray source was used at 50 kV and 200 mA, with 0.01° step widths, 1 s/step scans, and 1° glancing angles against the incident beam. In the FT-Raman measurements, an Ar laser with a wavelength of 514.5 nm and exciting laser power of 16 mW was used as the laser source.

Cross-sections of the samples were also observed under FE-SEM by the same methods described in a previous paper [24].

The scratch resistance of the surface layer formed on the alloys by the chemical and heat treatments was evaluated by measuring the critical load by which the layer was detached from the substrate using a thin-film scratch tester (CSR-2000, Rhesca Co. Ltd., Tokyo, Japan), using a stylus 5 μm in diameter and with a spring constant of 200 g mm⁻¹. Based on the standard JIS R-3255, the amplitude, scratch speed and loading rates were determined to be 100, 10 $\mu\text{m s}^{-1}$ and 100 mN min⁻¹, respectively. Five areas were scratched for each sample, and their average value was used in our analysis.

2.3 Soaking in SBF

The samples subjected to the chemical and heat treatments were soaked in 24 ml of SBF with ion concentrations (Na⁺ 142.0, K⁺ 5.0, Ca²⁺ 2.5, Mg²⁺ 1.5, Cl⁻ 147.8, HCO₃⁻ 4.2, HPO₄²⁻ 1.0, and SO₄²⁻ 0.5 mM) nearly equal to those of human blood plasma at 36.5°C. The SBF was prepared by dissolving reagent grade NaCl, NaHCO₃, KCl, K₂HPO₄·3H₂O, MgCl·6H₂O, CaCl₂, and Na₂SO₄ (Nacalai Tesque Inc., Kyoto, Japan) in ultrapure water, and buffered at pH = 7.4 with tris(hydroxymethyl)aminomethane (CH₂OH)₃CNH₂ and 1 M HCl (Nacalai Tesque Inc., Kyoto, Japan) at 36.5°C [25]. After soaking in the SBF for 3 days, the samples were removed, gently rinsed with ultrapure water for a period of 30 s, and dried at 40°C. Apatite formation on their surfaces was examined by TF-XRD, FE-SEM and EDX. To examine the stability of the apatite-forming ability, the treated alloy samples were incubated with a relative humidity of 95% at 80°C for 1 week. After removal from the incubator, their apatite-forming ability was examined by soaking in SBF for 3 days.

2.4 Measurement of mechanical properties

Rod samples which were 3 mm in diameter and 22 mm in length, as shown in Fig. 1, were prepared from the alloy (Toyota Central Research and Development Laboratories,

Inc.) for mechanical testing. Three rod samples as prepared and two rod samples which were subjected to the chemical and heat treatments were pulled at a speed of 1 mm min^{-1} using a tensile-testing machine (Servopulser EHF-L, Shimadu, Kyoto, Japan). Tensile strength, which is defined as the maximum load in the test, and 0.2% proof strength of the alloy samples were calculated from their stress–strain diagrams. Elongation of the alloy was estimated by measuring a change of guide length before and after the test. The reproducible results were obtained in the samples both before and after the chemical and heat treatments. A rod sample 5 mm in diameter and 60 mm in length with or without the chemical and heat treatments was prepared, and the elastic modulus of each sample was measured by the free vibration method (modified JE-RT, Nihon Techno-Plus Co. Ltd., Osaka, Japan).

2.5 Observation of microstructure

The rod samples used for the mechanical test were cut in the thread part perpendicular to a long axis, and their cross-sections were mirror finished using $0.05 \text{ }\mu\text{m}$ of alumina

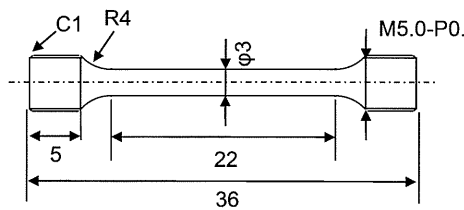


Fig. 1 Ti-36Nb-2Ta-3Zr-0.3O alloy rod for tensile test

powder followed by ultrasonic cleaning in acetone and ultrapure water for 10 min each. They were subjected to chemical etching using the diluted hydrofluoric acid with the composition of $\text{HF}:\text{HNO}_3:\text{H}_2\text{O} = 1:20:200$ to clarify their grain boundaries, washed by ultrapure water, and subjected to optical microscopic observation using trinocular metallurgical microscope (TMR-1, Yashima Optical Co. Ltd., Tokyo, Japan).

3 Results

3.1 Surface structures

Figure 2 shows the FE-SEM photographs of the surfaces and cross-sections of the Ti-36Nb-2Ta-3Zr-0.3O alloy which was untreated or treated with NaOH solution at different concentrations. It can be seen from Fig. 2 that a nano-sized network structure was formed uniformly on the surface of the alloy as a result of the 1 M NaOH treatment, whereas some cracks were formed by the treatments with the NaOH solutions at a higher concentration than 2 M, and both their numbers and size in width increased with increasing concentrations of the NaOH solution. It can be seen from the cross-sectional views that the thickness of the surface layer formed by the 1 M NaOH treatment was approximately 300 nm, and increased with increasing concentrations of the NaOH solution. With increasing thickness of the surface layer, cracks were formed in the surface layer because larger volume of the surface layer shrunk during drying process. Based on these results, 1 M

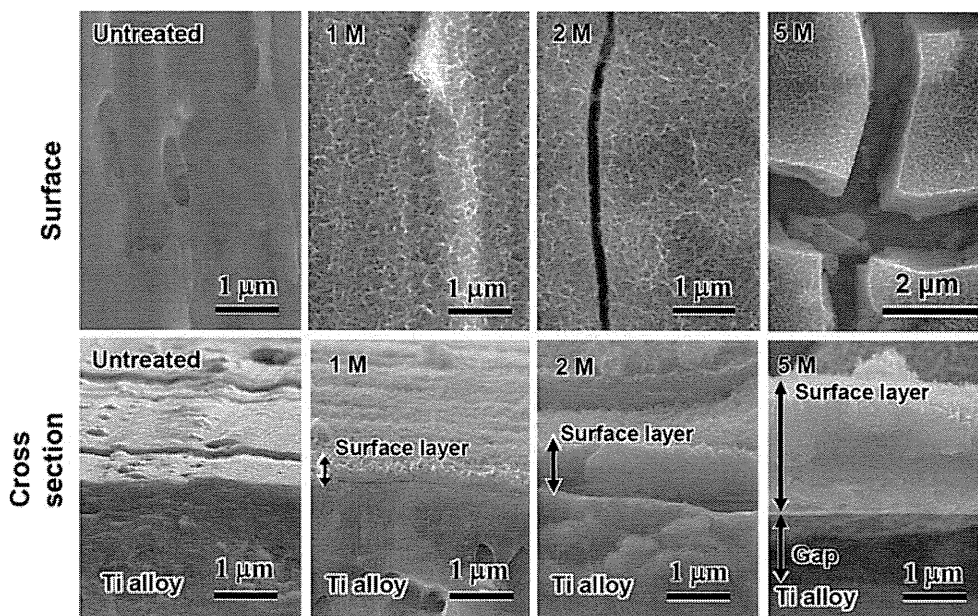


Fig. 2 FE-SEM photographs of the surfaces and cross sections of Ti-36Nb-2Ta-3Zr-0.3O alloy untreated and treated with 1, 2 or 5 M NaOH aqueous solutions

was selected as the concentration for the NaOH treatment in the following experiments.

Figure 3 shows the FE-SEM photographs of the surfaces of the alloys subjected to various heat treatment temperatures after the 1 M NaOH treatment, those subjected to heat treatments after the 1 M NaOH and the subsequent CaCl₂ treatment, and those finally subjected to the hot water treatment. It can be seen from the Fig. 3 that the nano-sized network structure formed by the NaOH treatment changed into granular structure when the alloy was heat-treated above 700°C without the subsequent CaCl₂ treatment, whereas the network morphology was maintained, even if it was heat-treated at 800°C, if the sample was soaked in CaCl₂ solution after the 1 M NaOH treatment. The water treatment after the heat treatment did not result in an apparent change in the surface morphologies.

Table 1 shows the results of the EDX analysis of the surfaces of the alloys subjected to the various solutions and heat treatments. Approximately 4.8 at.% of the sodium ions were incorporated into the surface of the alloy by the NaOH treatment. The amount of the sodium ions was not changed by the heat treatments up to 700°C, but was significantly decreased by the heat treatments above 800°C, where the niobium content increased. When the alloy sample was subjected to the CaCl₂ treatment after the 1 M NaOH treatment, the incorporated sodium ions were

completely replaced with calcium ions. The amount of calcium ions was not changed by the heat treatments up to 700°C, but was decreased by the heat treatments above 800°C. The subsequent water treatment slightly decreased the amount of calcium ions, regardless of the heat treatment temperature.

Figure 4 shows an AES depth profile of the surface of the alloy subjected to the 1 M NaOH–CaCl₂–heat700–water treatments. It can be seen from Fig. 4 that calcium and oxygen penetrated into the surface layer at depths of 300 and 500 nm, respectively. Both of these showed a gradual decrease with increasing depth, accompanied by a local maximum and minimum of approximately 150 nm in depth. In contrast, titanium and niobium showed a gradual increase with increasing depth. They also had a local minimum and maximum of approximately 150 nm in depth, respectively. These local maxima of calcium and niobium imply that some of the calcium niobates developed in a deep region of the surface layer.

Figure 5 shows the TF-XRD and FT-Raman profiles of the alloy surfaces left untreated and subjected to heat treatment at various temperatures after 1 M NaOH treatment. The broad FT-Raman peaks around 280, 450, 700, 820 and 910 cm⁻¹ in terms of the wave number appeared after the NaOH treatment, and they were matched with those of sodium hydrogen titanate (Na_xH_{2-x}Ti₃O₇)

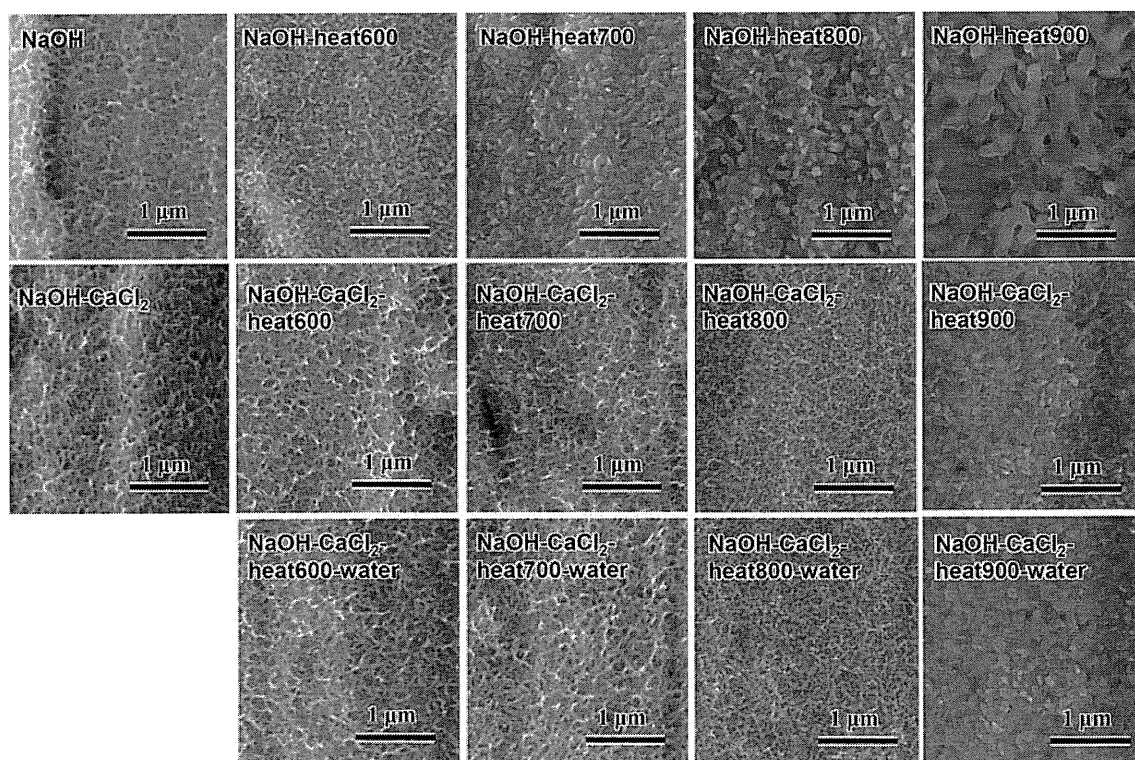
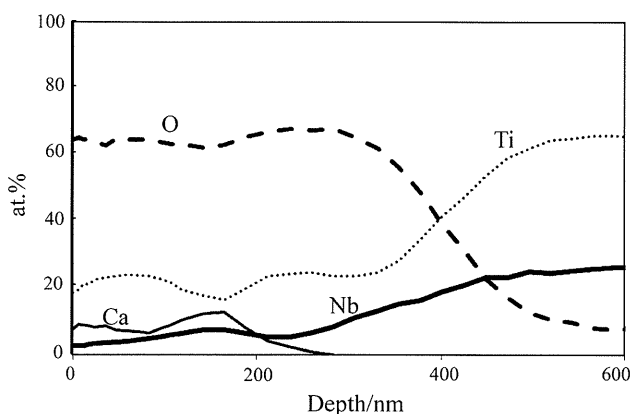


Fig. 3 FE-SEM photographs of the surfaces of Ti-36Nb-2Ta-3Zr-0.3O alloy subjected to heat treatment at various temperatures after 1 M NaOH treatment, or 1 M NaOH and CaCl₂ treatment, and those finally subjected to water treatment

Table 1 Results of EDX analysis of surface of Ti–36Nb–2Ta–3Zr–0.3O alloy untreated and subjected to 1 M NaOH, CaCl₂, heat at various temperature, and water treatments

Treatment	Elements (at.%)						
	O	Ti	Na	Ca	Nb	Ta	Zr
Untreated	11.9	67.9	0	0	18.4	0.5	1.4
1 M NaOH	57.6	32.9	4.8	0	5.2	0.1	0.3
1 M NaOH–heat600	50.3	40.7	4.3	0	4.3	0.1	0.4
1 M NaOH–heat700	57.2	34.1	4.6	0	3.8	0.1	0.3
1 M NaOH–heat800	59.5	30.5	2.5	0	7.3	0.1	0.2
1 M NaOH–heat900	59.1	29.5	0.4	0	10.9	0.1	0.1
1 M NaOH–CaCl ₂	52.9	37.4	0	5.2	4.0	0.1	0.3
1 M NaOH–CaCl ₂ –heat600	54.1	36.2	0	5.5	3.9	0.1	0.3
1 M NaOH–CaCl ₂ –heat600–water	57.0	33.9	0	4.6	4.0	0.1	0.4
1 M NaOH–CaCl ₂ –heat700	54.0	36.3	0	5.5	3.8	0.1	0.3
1 M NaOH–CaCl ₂ –heat700–water	54.9	36.5	0	4.6	3.7	0.1	0.3
1 M NaOH–CaCl ₂ –heat800	56.0	35.5	0	4.4	3.8	0.1	0.4
1 M NaOH–CaCl ₂ –heat800–water	57.0	34.8	0	3.9	3.8	0.1	0.4
1 M NaOH–CaCl ₂ –heat900	57.2	37.1	0	1.5	4.0	0.0	0.2
1 M NaOH–CaCl ₂ –heat900–water	56.9	37.4	0	1.4	4.0	0.0	0.3

**Fig. 4** Auger depth profile of Ti–36Nb–2Ta–3Zr–0.3O alloy subjected to 1 M NaOH, CaCl₂ heat700, and water treatments

reported in the literatures [26, 27]. The sodium hydrogen titanate was transformed into sodium titanate, Na₂Ti₆O₁₃ [26, 27], and rutile by the subsequent heat treatment up to 800°C, meanwhile sodium niobate (NaNbO₃), niobium oxide (Nb₂O₅) and rutile were precipitated by the heat treatment at 900°C. α -Ti with a peak position of around 40° in 2θ was detected besides β -Ti after the heat treatment at 600–800°C, indicating that phase transformation from β to α started in the alloy.

Figure 6 shows the TF-XRD and FT-Raman profiles of the alloy surfaces which were untreated and subjected to heat treatment at various temperatures after 1 M NaOH and CaCl₂ treatments and finally subjected to water treatment. When the alloy sample was soaked in CaCl₂ solution after the NaOH treatment, the FT-Raman peaks for sodium hydrogen titanate were almost unchanged, indicating that

the sodium hydrogen titanate was isomorphously transformed into calcium hydrogen titanate, Ca_xH_{2–2x}Ti₃O₇, by substituting the sodium ions with calcium ions. The calcium hydrogen titanate was transformed into calcium titanate, for which the phases were assumed to be CaTi₄O₉ including CaTi₂O₄ and CaTi₂O₅ [16, 28–30], anatase, and rutile, when it was heat-treated at 600°C. In contrast, the strong peak at around 31° of CaTi₂O₅, and weak peaks of 51° and 52° of Ca₂Nb₂O₇ in 2θ appeared in addition to the above peaks by the heat treatment at 700°C. These peaks gradually decreased when the heating temperature increased above 800°C, whereas the peaks attributed to Nb₂O₅ and CaNb₂O₆ were developed further with the increasing temperature of the heat treatment. These phases were not changed by the subsequent water treatment.

Table 2 shows the scratch resistance of the alloy subjected to the NaOH, CaCl₂, heat and water treatments. The scratch resistance of the surface layer formed by the initial NaOH treatment was as low as 7 mN. It increased markedly to approximately 61 mN by the heat treatment at 600°C, and increased with the increasing temperature of the heat treatment up to 800°C, but then was decreased slightly by the heat treatment at 900°C. The decrease of the scratch resistance by the heat treatment at 900°C might be due to the peeling of the thickened oxide layer. When the NaOH-treated alloy was subjected to the CaCl₂ treatment, its low scratch resistance was not changed. However, it was increased markedly to above 65 mN, by the subsequent heat treatment, similarly to the heat treatment after the NaOH treatment. The high scratch resistance was maintained even after the final water treatment.

Fig. 5 TF-XRD and FT-Raman profiles of the surfaces of Ti–36Nb–2Ta–3Zr–0.3O alloy subjected to heat treatment at various temperatures after 1 M NaOH treatment. *TA* α -titanium, *TB* β -titanium, *SHT* sodium hydrogen titanate ($\text{Na}_x\text{H}_{2-x}\text{Ti}_3\text{O}_7$), *filled inverted triangle* sodium titanate ($\text{Na}_2\text{Ti}_6\text{O}_{13}$), *R* rutile, *filled square* niobium oxide (Nb_2O_5), *SN* sodium niobate (NaNbO_3)

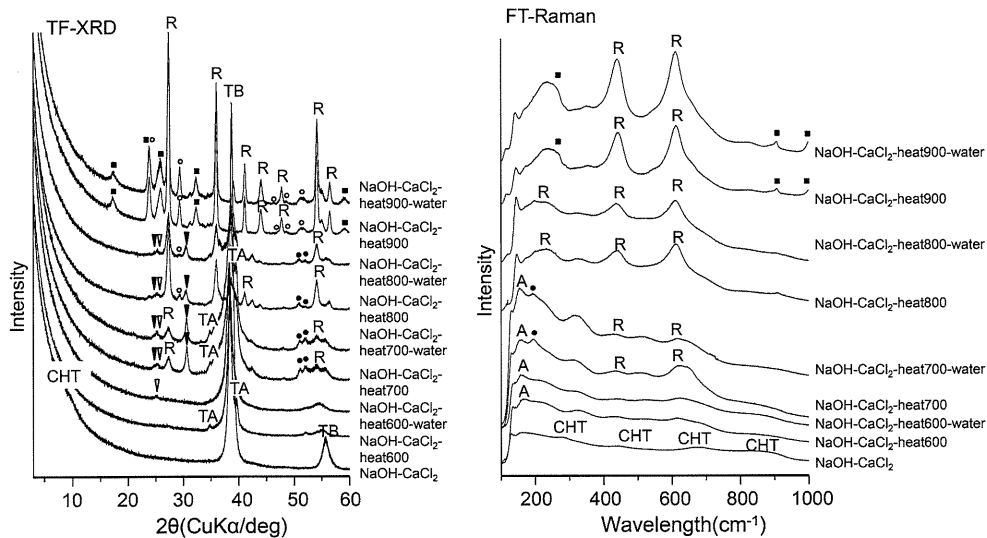
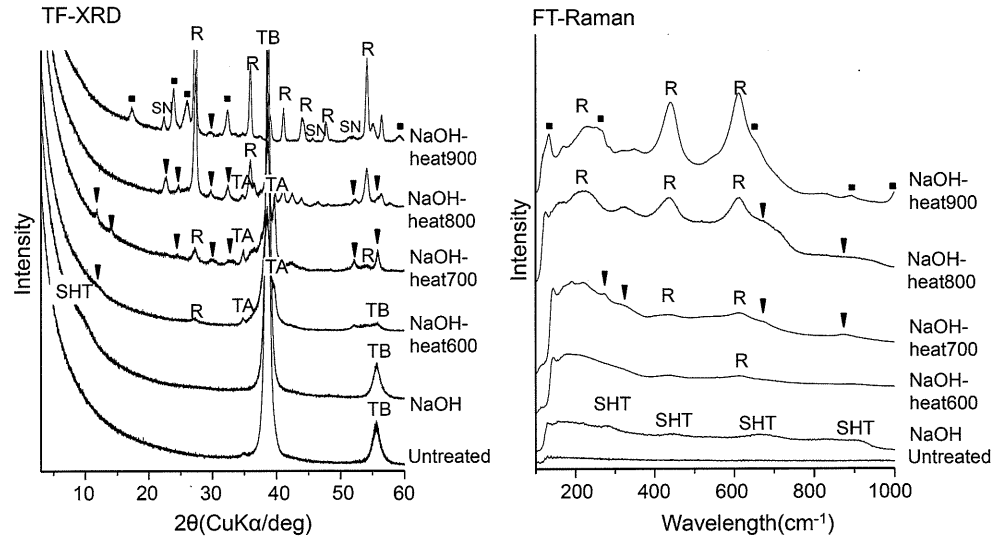


Fig. 6 TF-XRD and FT-Raman profiles of the surfaces of Ti–36Nb–2Ta–3Zr–0.3O alloy treated with 100 mM CaCl_2 aqueous solution after the NaOH treatment, and then subsequently subjected to heat treatment at various temperature and water treatment. *TA* α -titanium, *TB* β -titanium, *CHT* calcium hydrogen titanate ($\text{Ca}_x\text{H}_{2-2x}\text{Ti}_3\text{O}_7$), *open inverted triangle* calcium titanate (CaTi_4O_9), *filled inverted triangle* calcium titanate (CaTi_2O_5), *filled circle* calcium niobate (CaNb_2O_7), *open circle* calcium niobate (CaNb_2O_6), *filled square* niobium oxide (Nb_2O_5), *R* rutile, *A* anatase

3.2 Apatite formation

Figure 7 shows the FE-SEM photographs of the alloy surfaces soaked in SBF for 3 days after the NaOH, CaCl_2 , heat and water treatments. It can be seen from Fig. 7 that the alloy formed spherical precipitates on their surfaces, which were identified as crystalline apatite by TF-XRD given in Fig. 8, only when subjected to the NaOH, CaCl_2 , heat and water treatments. The amount of apatite formed on the alloy was strongly dependent on the temperature of the heat treatment, with the heat treatment at 700°C yielding the largest amount.

Figure 9 shows the FE-SEM photographs of the alloy surfaces soaked in SBF for 3 days after incubation under

95% humidity at 80°C for 1 week, following the 1 M NaOH– CaCl_2 –heat700–water treatments. The apatite-forming ability of the treated alloy was maintained even after the incubation, indicating the long-term stability of the apatite-forming ability in a humid environment at high temperature.

3.3 Mechanical properties

Figure 10 shows the typical stress–strain curves of the rod samples of the present alloy which was untreated and subjected to the 1 M NaOH– CaCl_2 –heat700–water treatments. It can be seen from Fig. 10 that the untreated rod samples display approximately 880 MPa of 0.2% proof

Table 2 Scratch resistance of Ti–36Nb–2Ta–3Zr–0.3O alloy subjected to 1 M NaOH, CaCl₂, heat at various temperature, and water treatments

Treatment	Scratch resistance (mN)	
	Average	Standard deviation
1 M NaOH	7.4	3.9
1 M NaOH-heat600	61.3	9.4
1 M NaOH-heat700	91.4	17.4
1 M NaOH-heat800	176.4	10.8
1 M NaOH-heat900	111.8	7.9
1 M NaOH–CaCl ₂	9.3	3.1
1 M NaOH–CaCl ₂ -heat600	65.8	14.4
1 M NaOH–CaCl ₂ -heat600–water	68.7	18.0
1 M NaOH–CaCl ₂ -heat700	104.5	20.5
1 M NaOH–CaCl ₂ -heat700–water	97.1	13.7
1 M NaOH–CaCl ₂ -heat800	194.4	1.6
1 M NaOH–CaCl ₂ -heat800–water	187.6	9.5
1 M NaOH–CaCl ₂ -heat900	123.3	9.6
1M NaOH–CaCl ₂ -heat900–water	134.4	6.5

strength, 1,030 MPa of tensile strength and 11% elongation. Elastic modulus measured by free vibration method was 65.4 GPa. These mechanical properties were only a little changed by the present treatment for inducing apatite formation, that is 798 MPa of 0.2% proof strength,

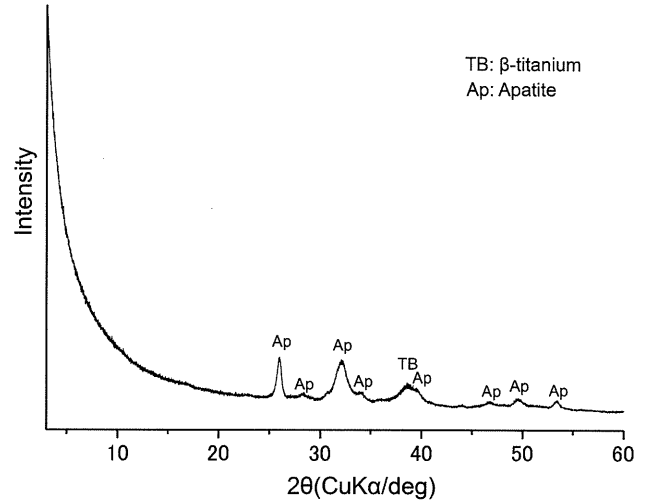


Fig. 8 TF-XRD profile of the surfaces of Ti–36Nb–2Ta–3Zr–0.3O alloy soaked in SBF for 3 days after the 1 M NaOH, CaCl₂, heat700 and water treatments

871 MPa of tensile strength, 10% elongation and 79.8 GPa of elastic modulus.

3.4 Microstructure

Figure 11 shows the metallurgical micrographs of the alloy samples untreated and subjected to the 1 M NaOH, CaCl₂,

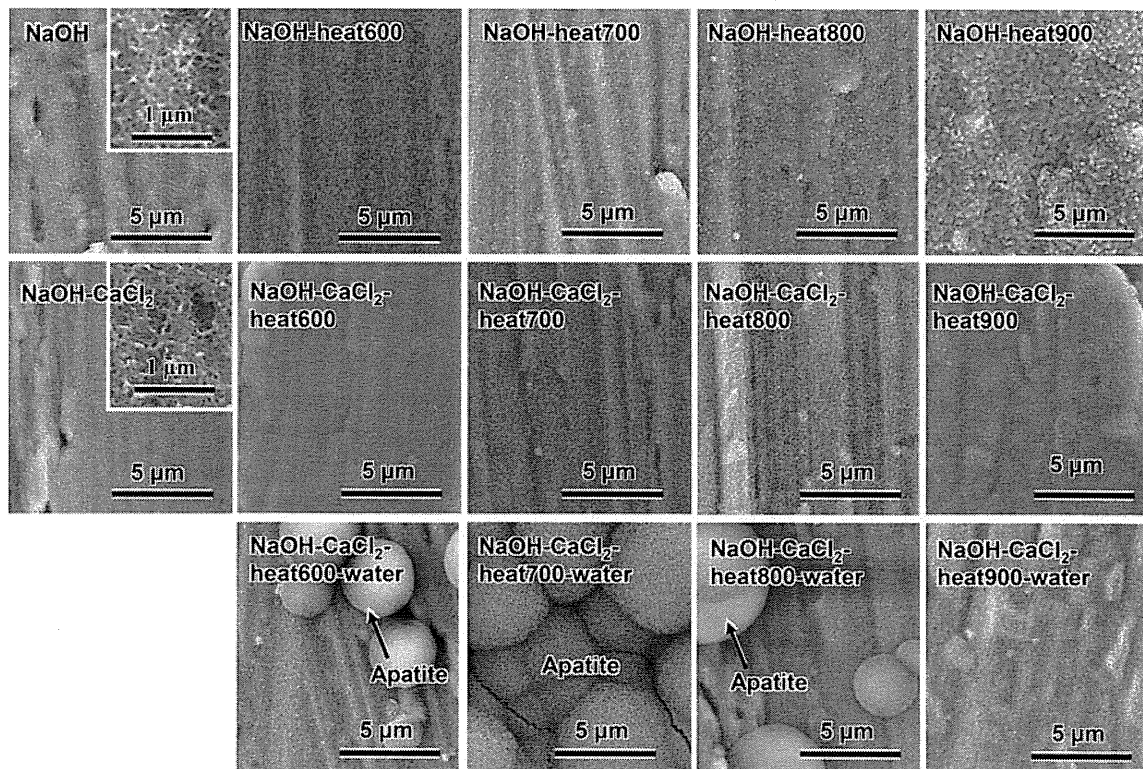


Fig. 7 FE-SEM photographs of the surfaces of Ti–36Nb–2Ta–3Zr–0.3O alloy soaked in SBF for 3 days after the NaOH, CaCl₂, heat at various temperatures and water treatments. *Inset* Photographs show high magnification

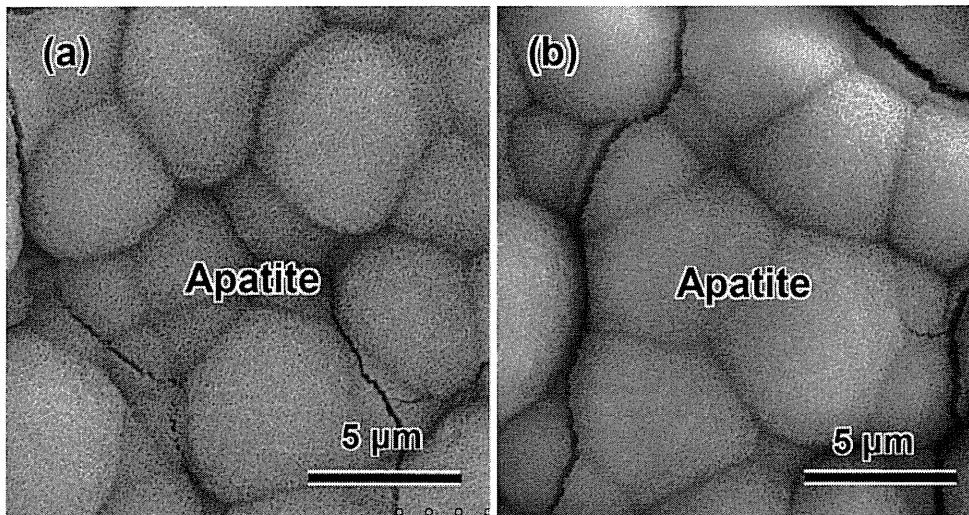


Fig. 9 FE-SEM photographs of the surfaces of Ti-36Nb-2Ta-3Zr-0.3O alloy soaked in SBF for 3 days **a** without and **b** with a storage under 95% humidity at 80°C for 1 week, following 1 M NaOH, CaCl₂, heat700, and water treatments

heat700 and water treatments. It can be seen from Fig. 11 that the sample took a homogeneous marble-like structure consisting of fine grains about 6 μm in width and several tens of μm in length before the treatments, while it was composed of circular large grains 10–50 μm in size accompanied by small grains after the treatments.

4 Discussion

It is apparent from Figs. 7 and 8 that high apatite formation in the Ti-36Nb-2Ta-3Zr-0.3O alloy is induced by the NaOH, CaCl₂, heat and water treatments, but can be induced by neither the simple NaOH plus heat treatments, nor the NaOH, CaCl₂ and heat treatments. The difference in the apatite-forming abilities between these surface

treatments is here discussed in terms of the surface structure.

A fine network layer that was approximately 300 nm in thickness was formed on the surface of the alloy by the NaOH treatment. This network consisted of nano-sized sodium hydrogen titanate, Na_xH_{2-x}Ti₃O₇. When the alloy thus treated was subsequently simply heat-treated, the sodium hydrogen titanate was transformed into sodium titanate, Na₂Ti₆O₁₃, and rutile at temperatures lower than 800°C. These surface structural changes of the present alloy are similar to those reportedly observed in pure titanium metal due to the NaOH and heat treatments [27]. In the case of the pure Ti metal, the treated metal forms apatite on its surface in SBF by the following mechanism. The sodium ions in the sodium titanate release via exchange with oxonium ions in SBF to form Ti-OH groups on the surface of the Ti metal [31, 32]. As a result, the pH of the surrounding SBF increases. The Ti-OH groups are negatively charged in the alkali solution [33] so as to combine with the positively charged calcium ions in SBF. As the calcium ions accumulate, the surface of the Ti metal is positively charged and combines with the negatively charged phosphate ions, forming the apatite [31, 32]. The reason the present alloy with the sodium titanate on its surface did not form the apatite in SBF might be attributed to the suppression of sodium ion release from the sodium titanate by the incorporated niobium ions, as in the case of the Ti-15Zr-4Nb-4Ta alloy [15].

When the present alloy was subjected to the CaCl₂ treatment after the NaOH treatment, the sodium hydrogen titanate formed by the NaOH treatment substituted the sodium ions with calcium ions to form a calcium hydrogen titanate, Ca_xH_{2-2x}Ti₃O₇, which takes a layered structure

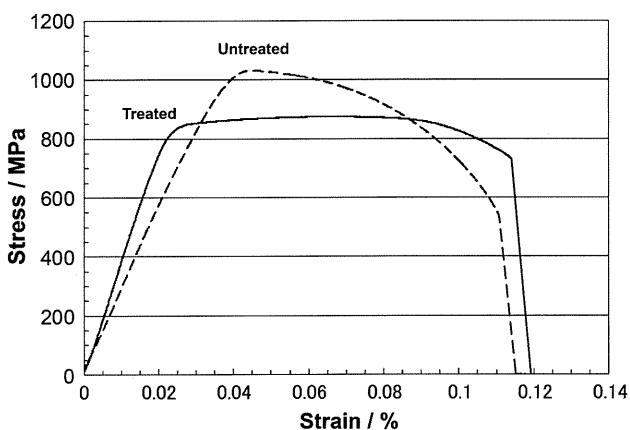


Fig. 10 Typical stress-strain curve of Ti-36Nb-2Ta-3Zr-0.3O with or without 1 M NaOH, CaCl₂, heat700 and water treatments

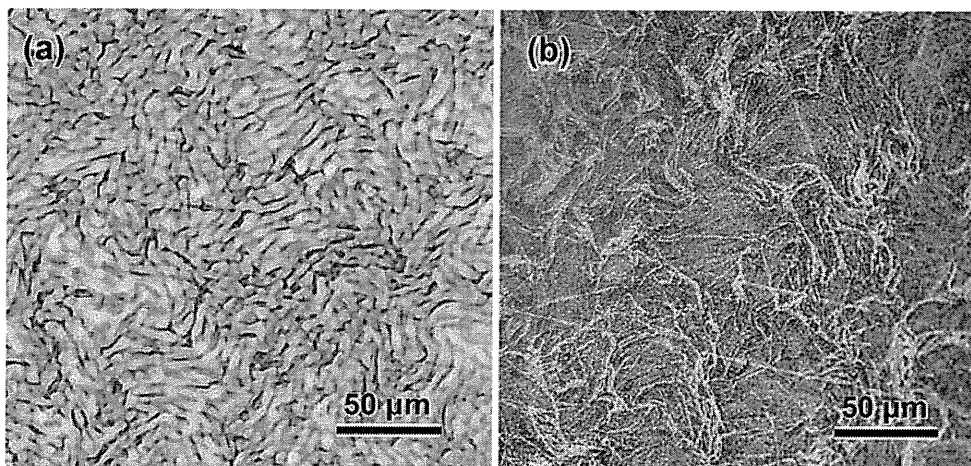


Fig. 11 Metallurgical micrographs of Ti-36Nb-2Ta-3Zr-0.3O alloy **a** untreated and **b** subjected to 1 M NaOH, CaCl₂, heat700 and water treatments

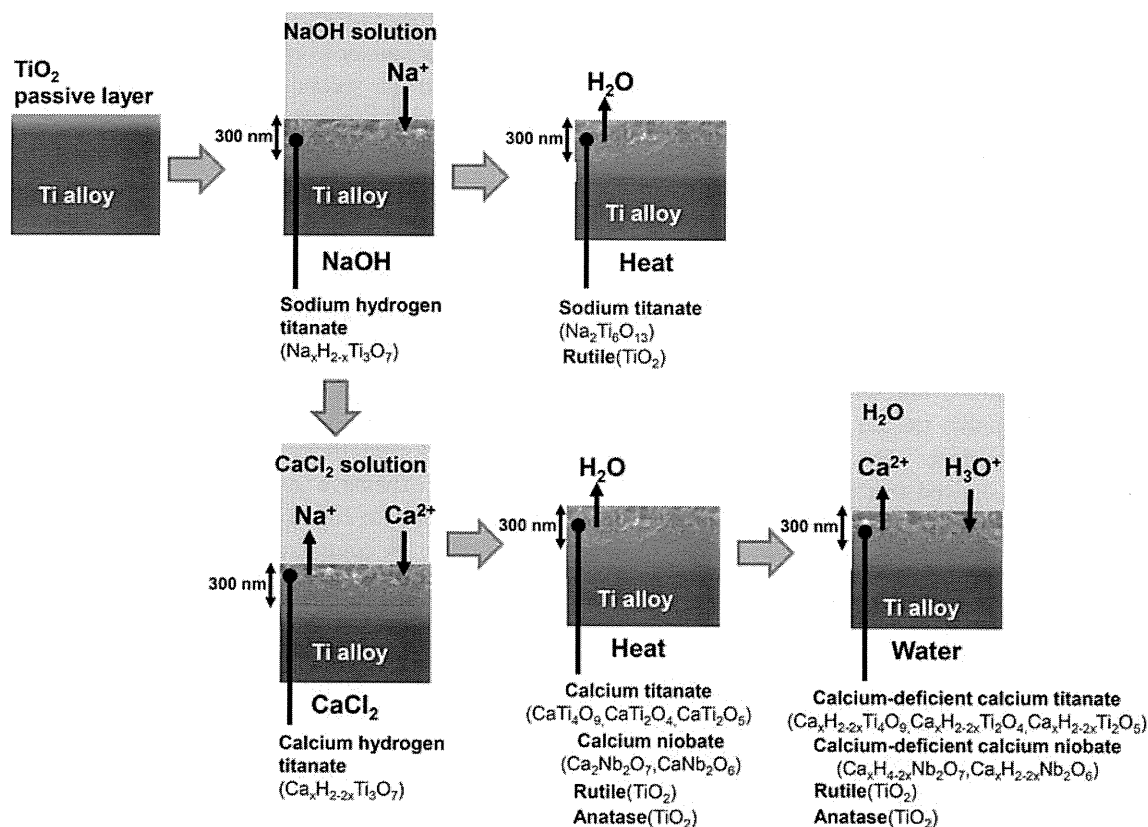


Fig. 12 Structural changes of the surfaces of Ti-36Nb-2Ta-3Zr-0.3O due to NaOH, CaCl₂, heat and water treatments

[34]. Thus, the formed calcium hydrogen titanate transformed into various forms of calcium titanate, such as CaTi₄O₉, CaTi₂O₄ and CaTi₂O₅, calcium niobate such as Ca₂Nb₂O₇ and CaNb₂O₆, rutile and anatase by the subsequent heat treatment, as is schematically shown in Fig. 12. None of the alloys treated in this manner formed apatite on their surfaces in SBF. This might be attributed to the extremely low diffusion constant of the calcium ions in

the formed calcium titanates and niobate, as in the case of the calcium titanate of Ti-15Zr-4Nb-4Ta alloy [16].

The final water treatment exchanged a portion of the calcium ions in the surface layer for oxonium ions without an apparent change in the crystal phases, as shown in Figs. 4 and 6. Thus, the resultant phases can be described as Ca_xH_{2-2x}Ti₄O₉, Ca_xH_{2-2x}Ti₂O₄ and Ca_xH_{2-2x}Ti₂O₅ for the calcium-deficient calcium titanate, and Ca_xH_{4-2x}Nb₂O₇

and $\text{Ca}_x\text{H}_{2-2x}\text{Nb}_2\text{O}_6$ for the calcium-deficient calcium niobate. The alloy treated thus exhibited a high capacity for apatite formation in SBF, as shown in Fig. 7. This might be due to the increased mobility of the calcium ions in the calcium titanates and niobates by incorporation of the some amounts of oxonium ions [16]. When the calcium ions are released from the calcium titanates and niobates in SBF, they promote apatite formation not only by the same mechanism as the sodium ions described above, but also by increasing ionic activity product of the apatite by the released calcium ions themselves.

However, it should be noted that thus induced apatite-forming ability was strongly dependent on the heat treatment temperature after the CaCl_2 treatment. The treated alloy showed the highest apatite-forming ability when it was heat-treated at 700°C . This could be attributed to the dominant precipitation of CaTi_2O_5 at around 700°C , as shown in Fig. 6. The calcium ions are more condensed in this compound than other calcium titanates such as CaTi_4O_9 , and hence are easily released in SBF.

The mobility of the calcium ions in the calcium titanate is, however, not so high that the calcium content is appreciably decreased in a humid environment. As a result, the high capacity for apatite formation conferred on the alloy by these treatments was maintained even after the incubation with 95% relative humidity at 80°C for at least 1 week. This is an important property in clinical applications, since medical devices are sometimes stored in humid condition for a long period of time before implantation.

In clinical applications, the scratch resistance of the chemically and thermally treated surface layer of the devices is also important. The experimental results described above also showed that the present alloy, after being subjected to the chemical and heat treatments so as to give high capacity for apatite formation, also exhibits high scratch resistance. It was experimentally confirmed that the high scratch resistance was maintained even after the incubation in humid condition.

It has been shown that Ti and various kinds of Ti-based alloys with the capacity to form apatite on their surfaces in SBF bond to living bone through the apatite layer formed on their surfaces in the living body [10, 11, 16, 17, 19–23]. In view of these findings, the present results indicate that the present alloy subjected to 1 M NaOH– CaCl_2 –heat700–water treatments is likely to tightly bond to living bone in the body.

Generally, the mechanical properties of Ti-based alloys are liable to be changed by chemical and heat treatments. It can be confirmed from Fig. 10 that the favorable mechanical properties of the present alloy, such as the low elastic modulus, high mechanical strength and large elastic deformation are only a little changed by the 1 M NaOH– CaCl_2 –heat700–water treatments. The slight decrease in

the proof strength from 880 to 798 MPa and slight increase in the elastic modulus from 65.4 to 79.8 GPa might be attributed to partial phase transformation of β -Ti to α -Ti in the alloy and their grain growth by the heat treatment after the chemical treatment, as shown in Figs. 6 and 11. Regardless of these small changes, the treated alloy still possesses higher mechanical strength and lower elastic modulus, which are favorable for orthopedic and dental implants, than Ti metal and conventional Ti alloy such as Ti–6Al–4V [35].

5 Conclusion

Ti–36Nb–2Ta–3Zr–0.3O alloy exhibits a high capacity for apatite formation in SBF when it was soaked in 1 M NaOH and 100 mM CaCl_2 solutions, heat-treated at 700°C , and soaked in water at 80°C . The first NaOH treatment forms sodium hydrogen titanate on the surface of the alloy, which serves as a precursor from which calcium hydrogen titanate is derived in the second CaCl_2 treatment. The third heat treatment transforms the calcium hydrogen titanate into calcium titanate predominately CaTi_2O_5 which exhibits high apatite formation in SBF after the subsequent hot water treatment which exchanges a portion of the calcium ions with oxonium ions. Thus, this capacity for high apatite formation was maintained even when the treated alloy was stored in a humid environment for a long period. The treated alloy also possesses a high level of scratch resistance, which is useful for clinical application. The sequential treatment in the present study consists of simple solution and heat treatments, which does not need any special and expensive apparatus, and is easily applied to large devices with complicated shapes. These features will be favorable for commercial manufacture.

The favorable mechanical properties of the present alloy, such as low elastic modulus, high mechanical strength and extensive elastic deformation are little changed by the surface treatment for inducing the apatite-forming ability. The present alloy conferred with high capacity for apatite formation is believed to be useful as unique materials for orthopedic and dental implants, since the treated alloy is expected to tightly bonds to bone in the living body and exhibit favorable mechanical properties.

References

1. Kokubo T, Miyaji F, Kim HM, Nakamura T. Spontaneous formation of bone-like apatite layer on chemically treated titanium metal. *J Am Ceram Soc.* 1996;79:1127–9.
2. Yan QW, Nakamura T, Kobayashi M, Kim HM, Kokubo T. Bonding of chemically treated titanium implants to bone. *J Biomed Mater Res.* 1997;37:267–75.

3. Wang XX, Hayakawa S, Tsuru K, Osaka A. Bioactive titania gel layers formed by chemical treatment of Ti substrate with a H_2O_2/HCl solution. *Biomaterials*. 2002;23:1353–7.
4. Wang XX, Yan W, Hayakawa S, Tsuru K, Osaka A. Apatite deposition on thermally and anodically oxidized titanium surfaces in a simulated body fluid. *Biomaterials*. 2003;24:4631–7.
5. Wu JM, Hayakawa S, Tsuru K, Osaka A. Low-temperature preparation of anatase and rutile layers on titanium substrates and their ability to induce in vitro apatite deposition. *J Am Ceram Soc*. 2004;87:1635–42.
6. Lu X, Wang Y, Yang X, Zhang Q, Zhao Z, Weng LT, Leng Y. Spectroscopic analysis of titanium surface functional groups under various surface modification and their behaviors in vitro and in vivo. *J Biomed Mater Res*. 2008;84A:523–34.
7. Sugino A, Ohtsuki C, Tsuru K, Hayakawa S, Nakano T, Okazaki Y, Osaka A. Effect of spatial design and thermal oxidation on apatite formation on Ti–15Zr–4Ta–4Nb alloy. *Acta Biomater*. 2009;5:298–304.
8. Karthega M, Rajendran N. Hydrogen peroxide treatment on Ti–6Al–4V alloy: a promising surface modification technique for orthopaedic application. *Appl Surf Sci*. 2010;256:2176–83.
9. Kawanabe K, Ise K, Goto K, Akiyama H, Nakamura T, Kaneuji A, Sugimori T, Mtsumoto T. Clinical device-related article a new cementless total hip arthroplasty with bioactive titanium porous-coating by alkaline and heat treatment: average 4.8-year results. *J Biomed Mater Res Part B*. 2009;90B:476–81.
10. Kim HM, Miyaji F, Kokubo T, Nakamura T. Preparation of bioactive Ti and its alloy via simple chemical surface treatment. *J Biomed Mater Res*. 1996;32:409–17.
11. Nishiguchi S, Nakamura T, Kobayashi M, Kim HM, Miyaji F, Kokubo T. Enhancement of bone-bonding strengths of titanium alloy implants by alkali and heat treatments. *J Biomed Mater Res (Appl Biomater)*. 1999;48:689–96.
12. Geetha M, Singh AK, Asokamani R, Gogia AK. Ti based biomaterials, the ultimate choice for orthopedic implants—a review. *Prog Mater Sci*. 2009;54:397–425.
13. Kawahara H, Ochi S, Tanetani K, Kato K, Isogai M, Mizuno H, et al. Biological testing of dental materials. *J Jpn Soc Dent Appar Mater*. 1963;4:65–75.
14. Okazaki Y, Rao S, Ito Y, Tateishi T. Corrosion resistance, mechanical properties, corrosion fatigue strength and cytocompatibility of new Ti alloys without Al and V. *Biomaterials*. 1998;19:1197–215.
15. Yamaguchi S, Takadama H, Matsushita T, Nakamura T, Kokubo T. Preparation of bioactive Ti–15Zr–4Nb–4Ta alloy from HCl and heat treatments after an NaOH treatment. *J Biomed Mater Res Part A*. 2011;97A:135–44.
16. Yamaguchi S, Takadama H, Matsushita T, Nakamura T, Kokubo T. Apatite-forming ability of Ti–15Zr–4Nb–4Ta alloy induced by calcium solution treatment. *J Mater Sci Mater Med*. 2010;21:439–44.
17. Fukuda A, Takemoto M, Saito T, Fujibayashi S, Neo M, Yamaguchi S, Kizuki T, Matsushita T, Niinomi M, Kokubo T, Nakamura T. Bone bonding bioactivity of Ti metal and Ti–Zr–Nb–Ta alloys with Ca ions incorporated on their surfaces by simple chemical and heat treatments. *Acta Biomater*. 2011;7:1379–86.
18. Saito T, Furuta T, Hwang JH, Kuramoto S, Nishino K, Suzuki N, Chen R, Yamada A, Ito Kazuhiko, Seno Y, Nonaka T, Ikehata H, Nagasako N, Iwamoto C, Ikuhara Y, Sakuma T. Multifunctional alloys obtained via a dislocation-free plastic deformation mechanism. *Science*. 2003;300:464–7.
19. Kim HM, Takadama H, Miyaji F, Kokubo T, Nishiguchi S, Nakamura T. Formation of bioactive functionally graded structure on Ti–6Al–4V alloy by chemical surface treatment. *J Mater Sci Mater Med*. 2000;11:555–9.
20. Kim HM, Takadama H, Kokubo T, Nishiguchi S, Nakamura T. Formation of a bioactive graded surface structure on Ti–15Mo–5Zr–3Al alloy by chemical treatments. *Biomaterials*. 2000;21:353–8.
21. Kizuki T, Takadama H, Matsushita T, Nakamura T, Kokubo T. Preparation of bioactive Ti metal surface enriched with calcium ions by chemical treatment. *Acta Biomater*. 2010;6:2836–42.
22. Nishiguchi S, Fujibayashi S, Kim HM, Kokubo T, Nakamura T. Biology of alkali- and heat- treated titanium implants. *J Biomed Mater Res*. 2003;67A:26–35.
23. Kokubo T, Pattanayak DK, Yamaguchi S, Takadama H, Matsushita M, Kawai T, Takemoto M, Fujibayashi S, Nakamura T. Positively charged bioactive Ti metal prepared by simple chemical and heat treatments. *J R Soc Interface*. 2010;7:S503–13.
24. Yamaguchi S, Takadama T, Matsushita T, Nakamura T, Kokubo T. Cross-sectional analysis of the surface ceramic layer developed on Ti metal by NaOH-heat treatment and soaking in SBF. *J Ceram Soc Jpn*. 2009;117:1126–30.
25. Kokubo T, Takadama H. How useful is SBF in predicting in vivo bone bioactivity? *Biomaterials*. 2006;27:2907–15.
26. Sun X, Li Y. Synthesis and characterization of ion-exchangeable titanate nanotubes. *Chem Eur J*. 2003;9:2229–38.
27. Kawai T, Kizuki T, Takadama H, Matsushita T, Kokubo T, Unuma H, Nakamura T. Apatite formation on surface titanate layer with different Na content on Ti metal. *J Ceram Soc Jpn*. 2010;9:19–24.
28. Joint Committee on Powder Diffraction Standards (JCPDS) Powder Diffraction Data File 00-026-0333.
29. Joint Committee on Powder Diffraction Standards (JCPDS) Powder Diffraction Data File 01-072-1134.
30. Joint Committee on Powder Diffraction Standards (JCPDS) Powder Diffraction Data File 00-025-1450.
31. Kim HM, Himeno T, Kawashita M, Lee JH, Kokubo T, Nakamura T. Surface potential change in bioactive titanium metal during the process of apatite formation in simulated body fluid. *J Biomed Mater Res*. 2003;67A:1305–9.
32. Takadama H, Kim HM, Kokubo T, Nakamura T. TEM-EDX Study of mechanism of bonelike apatite formation on bioactive titanium metal in simulated body fluid. *J Biomed Mater Res*. 2001;57:441–8.
33. Textor M, Sitting C, Franchiger V, Tosatti S, Brunette DM. Properties and biological significance of natural oxide films on titanium and its alloys. In: Brunette DM, Tengrall P, Textor M, Thomsen P, editors. Titanium in medicine. New York: Springer; 2001. p. 172–230.
34. Morgado E Jr, de Abreu MAS, Pravia ORC, Marinkovic BA, Jardim PM, Rizzo FC, Aroujo AS. A study on the structure and thermal stability of titanate nanotubes as a function of sodium content. *Solid State Sci*. 2006;8:888–900.
35. The Japan Institute of Metal. Metal data book: a fourth look. Tokyo: Maruzen; 2004. p. 256.

Apatite-forming ability of titanium in terms of pH of the exposed solution

Deepak K. Pattanayak, Seiji Yamaguchi, Tomiharu Matsushita, Takashi Nakamura and Tadashi Kokubo

J. R. Soc. Interface published online 14 March 2012

doi: 10.1098/rsif.2012.0107

References

This article cites 45 articles, 1 of which can be accessed free
<http://rsif.royalsocietypublishing.org/content/early/2012/03/08/rsif.2012.0107.full.html#ref-list-1>

P<P

Published online 14 March 2012 in advance of the print journal.

Email alerting service

Receive free email alerts when new articles cite this article - sign up in the box at the top right-hand corner of the article or click [here](#)

Advance online articles have been peer reviewed and accepted for publication but have not yet appeared in the paper journal (edited, typeset versions may be posted when available prior to final publication). Advance online articles are citable and establish publication priority; they are indexed by PubMed from initial publication. Citations to Advance online articles must include the digital object identifier (DOIs) and date of initial publication.

To subscribe to *J. R. Soc. Interface* go to: <http://rsif.royalsocietypublishing.org/subscriptions>

Apatite-forming ability of titanium in terms of pH of the exposed solution

Deepak K. Pattanayak¹, Seiji Yamaguchi¹, Tomiharu Matsushita¹,
Takashi Nakamura² and Tadashi Kokubo^{1,*}

¹*Graduate School of Biomedical Sciences, Chubu University, 1200 Matsumoto-cho,
Kasugai 487-8501, Japan*

²*Kyoto Medical Center, National Hospital Organisation, 1-1, Fukakusa Mukaihata-cho,
Fushimi-ku, Kyoto 612-8555, Japan*

In order to elucidate the main factor governing the capacity for apatite formation of titanium (Ti), Ti was exposed to HCl or NaOH solutions with different pH values ranging from approximately 0 to 14 and then heat-treated at 600°C. Apatite formed on the metal surface in a simulated body fluid, when Ti was exposed to solutions with a pH less than 1.1 or higher than 13.6, while no apatite formed upon exposure to solutions with an intermediate pH value. The apatite formation on Ti exposed to strongly acidic or alkaline solutions is attributed to the magnitude of the positive or negative surface charge, respectively, while the absence of apatite formation at an intermediate pH is attributed to its neutral surface charge. The positive or negative surface charge was produced by the effect of either the acidic or alkaline ions on Ti, respectively. It is predicted from the present results that the bone bonding of Ti depends upon the pH of the solution to which it is exposed, i.e. Ti forms a bone-like apatite on its surface in the living body and bonds to living bone through the apatite layer upon heat treatment after exposure to a strongly acidic or alkaline solution.

Keywords: titanium; NaOH or HCl treatments; apatite-forming ability; simulated body fluid; zeta potential; X-ray photoelectron spectroscopy

1. INTRODUCTION

Titanium (Ti) and its alloys are widely used in various types of implants in orthopaedic and dental fields, because of their good biocompatibility and high mechanical strength [1]. It is reported that they could have bonded to living bone after long-term implantation. However, they do not always bond to living bone, especially in a short period of time after implantation [2] and hence, their fixation in the living body is not always stable. Fast and reliable bonding to the bone is desirable for orthopaedic and dental implants. Various attempts have been made to induce bone bonding by techniques such as ion implantation [3–5], electrochemical [6–10] and hydrothermal treatment [11–15]. Certain chemical and heat treatments have also been attempted [16–21]. Improvement in bone bonding has been reportedly induced by these treatments. However, some reports have attributed the improvement to the surface roughness increased by the treatments, while others have pointed to the formation of specific crystalline phases such as anatase and rutile induced by the treatments. There is thus inadequate consistency in these interpretations, and the purpose of the present paper is to inquire into the main factor governing the bone-bonding properties of Ti.

We previously reported that Ti and its alloys spontaneously tightly bond to living bone when soaked in NaOH solution and then subjected to heat treatment [22–24]. These treatments have been applied to a porous Ti metal layer of an artificial hip joint, and the resulting bioactive hip joint has been used clinically in Japan since 2007 [25]. On the other hand, it was also shown that Ti spontaneously bonds to living bone when soaked in a H₂SO₄/HCl mixed acid solution and then subjected to heat treatment [26]. The bonding of the Ti subjected to NaOH and acid treatments to living bone has been attributed to surface apatite formation in the living body [24,26]. However, the dependence of this apatite formation on Ti metal upon the pH of the exposed solution has not been reported.

In the present study, Ti was exposed to simple aqueous solutions in which the pH was systematically changed from approximately 0 to 14 by HCl and NaOH solutions, and then subjected to a heat treatment. Surface apatite formation was examined in a simulated body fluid (SBF) using an ion concentration almost equal to that in human blood plasma [27], in comparison with those on Ti prior to heat treatment. The dependence of their apatite-forming ability on the pH of the solution is discussed in terms of surface roughness, the kind of the surface crystalline phase and the surface charges.

It has been shown that various kinds of bone-bonding bioactive ceramics have the capacity to form

*Author for correspondence (kokubo@isc.chubu.ac.jp).

2 *Apatite-forming ability of titanium* D. K. Pattanayak *et al.*

Table 1. pH of exposed solution.

solution	HCl				water	NaOH			
	5 M	1 M	100 mM	0.5 mM		0.5 mM	100 mM	1 M	5 M
pH	approx. 0	0.1	1.1	3.4	6–7	10.8	12.9	13.6	approx. 14

a surface apatite layer in SBF and to bond to living bone through this surface apatite layer *in vivo* [27]. The bone-bonding properties of Ti are discussed in terms of apatite-forming ability.

2. MATERIAL AND METHODS

2.1. Preparation of the samples

Commercially pure Ti (Grade no. 2; Kobe Steel, Ltd, Japan) was cut into rectangular samples having the dimensions of $10 \times 10 \times 1 \text{ mm}^3$, abraded with a no. 400 diamond plate, washed with acetone, 2-propanol and ultra pure water for 30 min each in an ultrasonic cleaner and then dried overnight in an oven at 40°C . Each specimen was soaked in 5 ml of HCl or NaOH solution at concentrations ranging from 0.5 mM to 5 M and water at 60°C in an oil bath, shaken at $120 \text{ strokes min}^{-1}$ for 24 h, and then washed with flowed ultra-pure water for 30 s. The washing time was carefully selected as the shortest time when any precipitations from surplus NaOH solution could not be detected on the specimen treated with the NaOH solution. The pH values of the solutions are given in table 1. The specimens removed from the solutions were heated to 600°C at a rate of 5°C min^{-1} in an Fe–Cr electric furnace under an ambient atmosphere, maintained at this temperature for 1 h and then cooled naturally to room temperature in the furnace.

2.2. Surface analysis of the treated Ti metals

The surface of the Ti specimens treated as described in §2.1 was analysed using thin-film X-ray diffraction (TF-XRD, RINT-2500, Rigaku Co., Japan). The X-ray source was $\text{CuK}\alpha$, and the angle of the incident beam was set to 1° against the sample surface.

The same surface was coated with a Pt/Pd film and observed under field emission scanning electron microscopy (FE-SEM, Hitachi S-4300, Hitachi, Japan).

The depth profiles of various elements near the surface of the Ti specimens subjected to the acid and heat treatments were analysed using radio frequency (RF) glow discharge optical emission spectroscopy (GD-OES, GD-Profilier 2, Horiba Co., Japan) under Ar sputtering at an Ar pressure of 600 Pa. An RF electric field with a power of 35 W was applied at a regular interval of 20 ms.

Ti plates having the dimensions of $13 \times 33 \times 1 \text{ mm}^3$ were prepared for measurement of the zeta potential, where the volume of the NaOH and HCl solutions and water for the surface treatments was increased to 20 ml. The Ti specimens soaked in the solutions and then heat-treated were electrically grounded to discharge any stray charges, and were immediately placed in the zeta potential and particle size analyser

(ELS-Z1, Otsuka Electronics Co., Japan) using a glass cell for the plate sample. The zeta potential of the specimens was measured under an applied voltage of 40 V in 10 or 50 mM NaCl solution dispersing monitor particles of polystyrene latex particles (diameter = 500 nm) coated with hydroxyl propyl cellulose. When 40 V of the voltage was applied, the flow of electro-osmosis depending on the surface charge of the specimens was generated. The zeta potential was calculated from the distribution of the flow of electro-osmosis by monitoring the migration velocity of the monitor particles. Five samples were measured for each experimental condition, and the average value was used in the analysis.

2.3. Examination of the apatite formation in an simulated body fluid

The Ti specimens treated as described earlier were soaked in 30 ml of an acellular SBF at 36.5°C with ion concentrations ($\text{Na}^+ = 142.0$, $\text{K}^+ = 5.0$, $\text{Mg}^{2+} = 1.5$, $\text{Ca}^{2+} = 2.5$, $\text{Cl}^- = 147.8$, $\text{HCO}_3^- = 4.2$, $\text{HPO}_4^{2-} = 1.0$, and $\text{SO}_4^{2-} = 0.5 \text{ mM}$) nearly equal to those in human blood plasma. The SBF was prepared by dissolving reagent-grade NaCl, NaHCO_3 , KCl, $\text{K}_2\text{HPO}_4 \cdot 3\text{H}_2\text{O}$, $\text{MgCl}_2 \cdot 6\text{H}_2\text{O}$, CaCl_2 and Na_2SO_4 (Nacalai Tesque Inc., Japan) in ultra-pure water, and buffered at $\text{pH} = 7.40$ using tris (hydroxymethyl) aminomethane $[(\text{CH}_2\text{OH})_3\text{CNH}_2]$ and 1 M HCl (Nacalai Tesque Inc.) [27].

After soaking in the SBF for 3 days, the surface was analysed for apatite formation with TF-XRD and FE-SEM using the methods described in §2.2.

The surfaces of the Ti specimens treated as described in §2.1 and soaked in SBF for various periods were analysed using X-ray photoelectron spectroscopy (XPS, ESCA-3300KM, Shimadzu Co., Japan), with $\text{MgK}\alpha$ radiation ($\lambda = 9.8903 \text{ \AA}$) as the X-ray source. The XPS take-off angle was set at 45° , which enabled the system to detect photoelectrons to a depth of 5–10 nm from the surface of the substrate. The binding energy of the measured spectra was calibrated by reference to the C_{1s} peak of the surfactant CH_2 groups on the substrate occurring at 284.6 eV.

3. RESULTS

3.1. Surface structure of the treated Ti metal

Figure 1 shows the FE-SEM micrographs of the surface of Ti specimens exposed to solutions with the different pHs, and also those that were subsequently heat-treated. Cross-sectional photographs of the Ti specimens exposed to solutions with the low or high pHs and subsequently heat-treated are also shown. It can be seen from figure 1 that a ripple-like micrometre scale roughness was formed on the Ti surface by exposure to solutions with

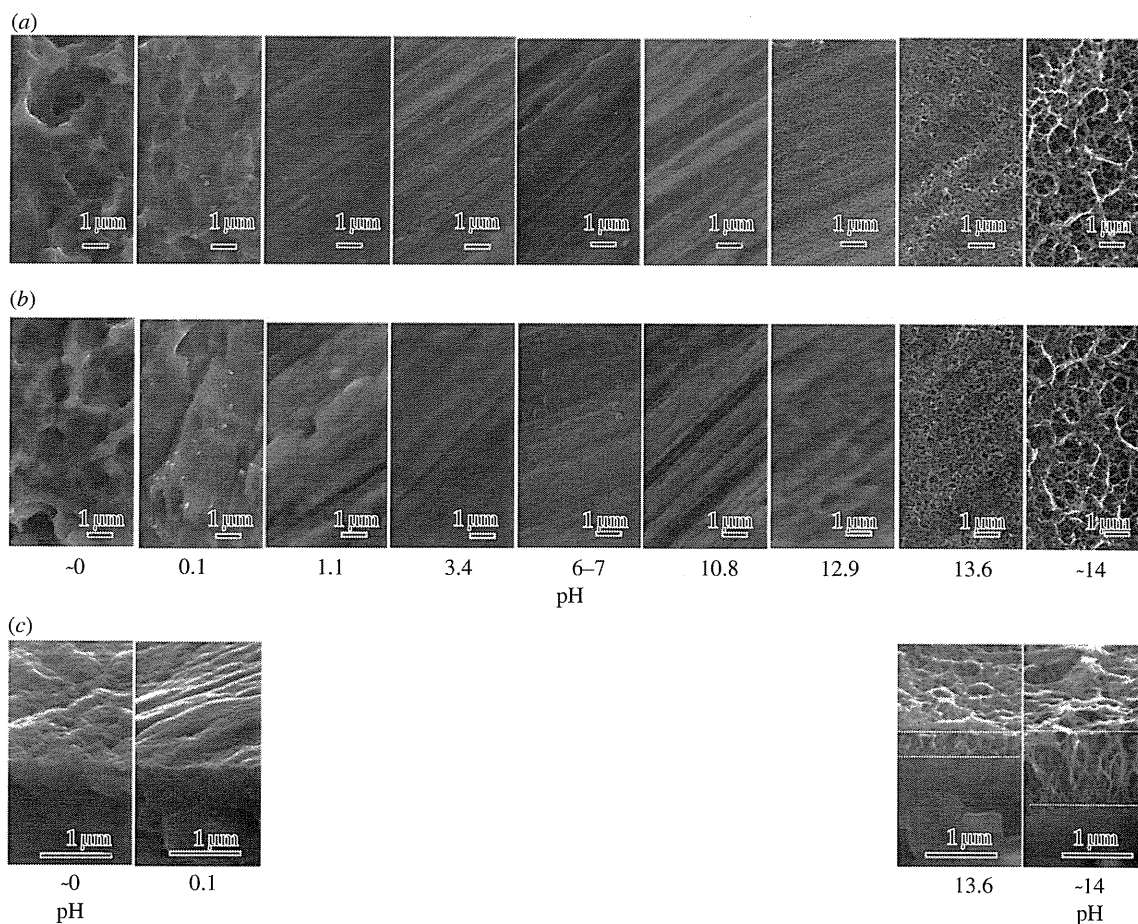


Figure 1. (a) Before and (b) after heat treatment. FE-SEM photographs of surfaces of Ti as exposed to solutions with different pHs, and those subsequently subjected to heat treatment. (c) Cross-sectional photographs of Ti metals exposed to solutions with low and high pHs and subsequently heat-treated are given at the bottom.

a pH lower than 0.1, while a nanometre scale roughness consisting of a network of feather-like phases that were elongated perpendicularly to the surface was formed on the Ti surface by exposure to solutions with a pH higher than 13.6. The Ti surface morphology was not changed by exposure to solutions with intermediate pHs ranging from 1.1 to 12.9. None of these topographies were essentially changed by the subsequent heat treatment.

Figure 2 shows TF-XRD patterns of the surfaces of the Ti specimens exposed to solutions with the different pHs, and also those that were subsequently heat-treated. It can be seen from figure 2 that titanium hydride (TH; TiH_x) [26] or sodium hydrogen titanate (SHT; $\text{Na}_x\text{H}_{2-x}\text{Ti}_3\text{O}_7$, $0 < x < 2$) [28] formed on the surface of Ti when treated with solutions of pH values lower than 0.1 or higher than 13.6, respectively. After the subsequent heat treatment, all the Ti specimens formed a titanium oxide of rutile phase irrespective of the pH of the solution. Only the pH values higher than 13.6 resulted in the formation of sodium titanate ($\text{Na}_2\text{Ti}_6\text{O}_{13}$) in addition to rutile after the heat treatment.

3.2. Zeta potential of the treated Ti metal

The zeta potential of a metal specimen with no electrically insulating oxide layer or one that was too thin

cannot be measured by the present method, and hence the Ti specimens as exposed to the solutions could not be measured, because no or only a very thin oxide layer exists on their surfaces. This suggests that their zeta potentials are almost zero.

The zeta potentials of the Ti specimens subjected to the heat treatment after exposure to the solutions is shown in figure 3 as a function of the solution pH. Ti specimens exposed to solutions with a pH lower than 1.1 displayed a positive zeta potential higher than 5 mV, whereas those exposed to solutions with a pH higher than 13.6 displayed a negative zeta potential less than -10 mV. Those exposed to solutions with intermediate pH values that ranged from 3.4 to 12.9 had a zeta potential of approximately zero.

3.3. Distribution of elements near the surface

Figure 4 shows the depth profile of the GD-OES spectra of Ti specimens exposed to the solution with a pH ~ 0 and also those that were subsequently subjected to heat treatment, as a function of sputtering time. Large amounts of H and O besides Ti were detected in the surface layer of the specimen exposed to the acid solution because of the formation of TH and titanium oxide by the acid treatment. It should be noted here that a small amount of Cl was also detected on its surface layer.

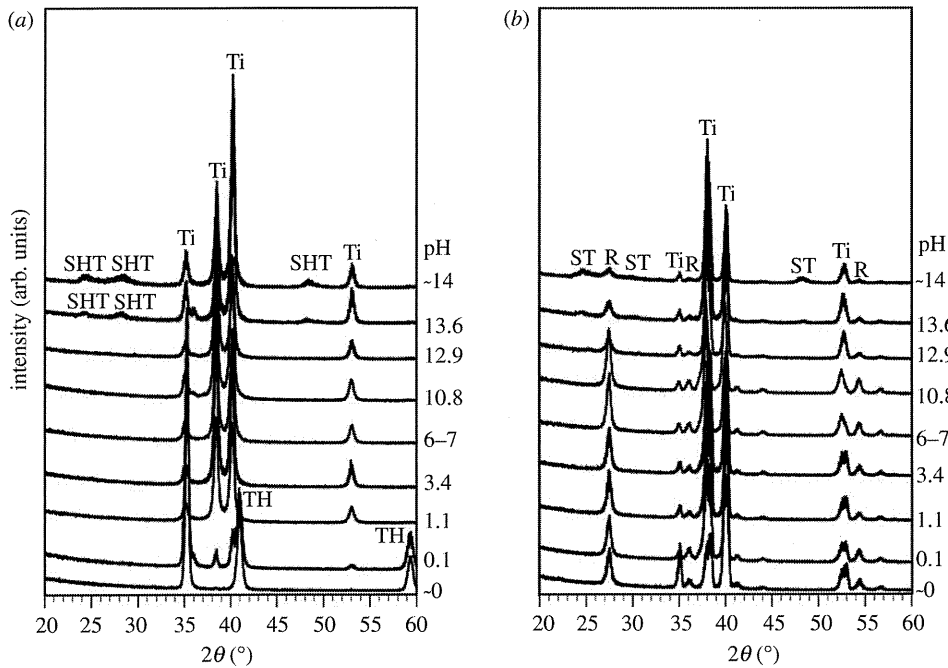


Figure 2. (a) Before and (b) after heat treatment. TF-XRD patterns of surfaces of Ti as exposed to solutions with different pHs, and those subsequently subjected to heat treatment. Ti, α Ti; TH, titanium hydride; SHT, sodium hydrogen titanate; ST, sodium titanate; R, rutile.

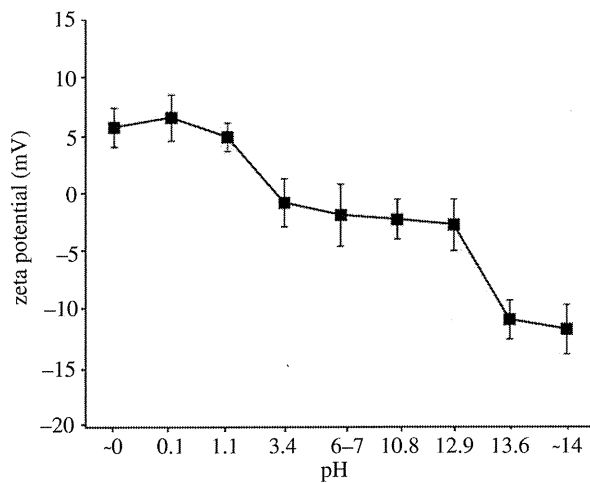


Figure 3. Zeta potentials of Ti as exposed to solutions with different pHs and subsequently subjected to heat treatment.

The results show that H was remarkably reduced, while O was increased by the heat treatment because of transformation of the TH to titanium oxide. It should be noted here once again that a small amount of Cl was detected even after the heat treatment.

Depth profiles of elements near the surfaces of Ti specimens exposed to the NaOH solution with pH \sim 14 and those that were subsequently subjected to heat treatment were previously examined by Auger electron spectroscopy and already published [29]. According to the result, Na and O penetrated into the Ti specimen up to a depth of about 1 μ m as a result of the NaOH treatment and their concentrations gradually decreased

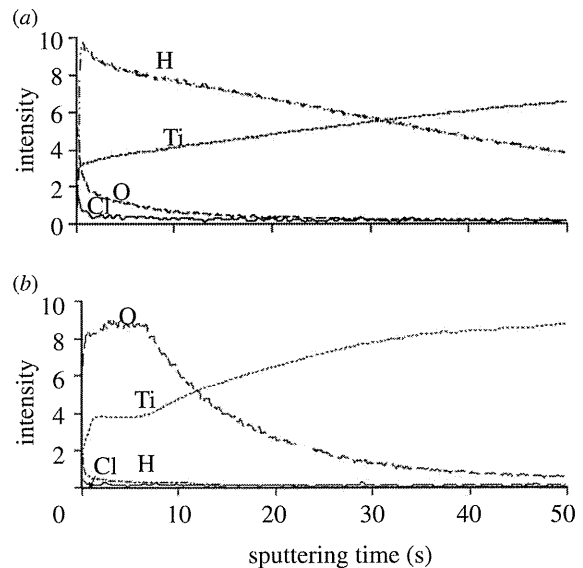


Figure 4. (a) Before and (b) after heat treatment. Depth profile of GD-OES spectra of surfaces of Ti as-exposed to the solutions with pH \sim 0 and that subsequently subjected to heat treatment, as a function of sputtering time.

with increasing depth. Only O penetrated into a deeper region, while Na did not show any change in its distribution by the subsequent heat treatment.

3.4. Apatite-forming ability of treated Ti metal in simulated body fluid

The FE-SEM micrographs in figure 5 show the surface of the Ti specimens soaked in SBF for 3 days after

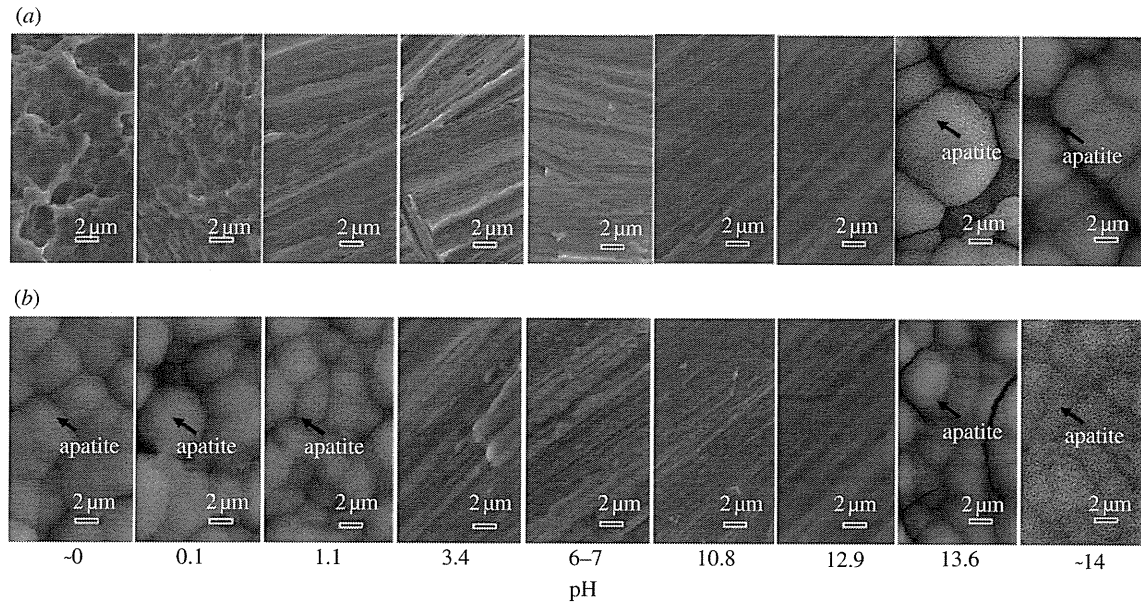


Figure 5. (a) Before and (b) after heat treatment. FE-SEM photographs of surfaces of Ti soaked in SBF for 3 days after exposure to solutions with different pHs, and those after subsequent heat treatment.

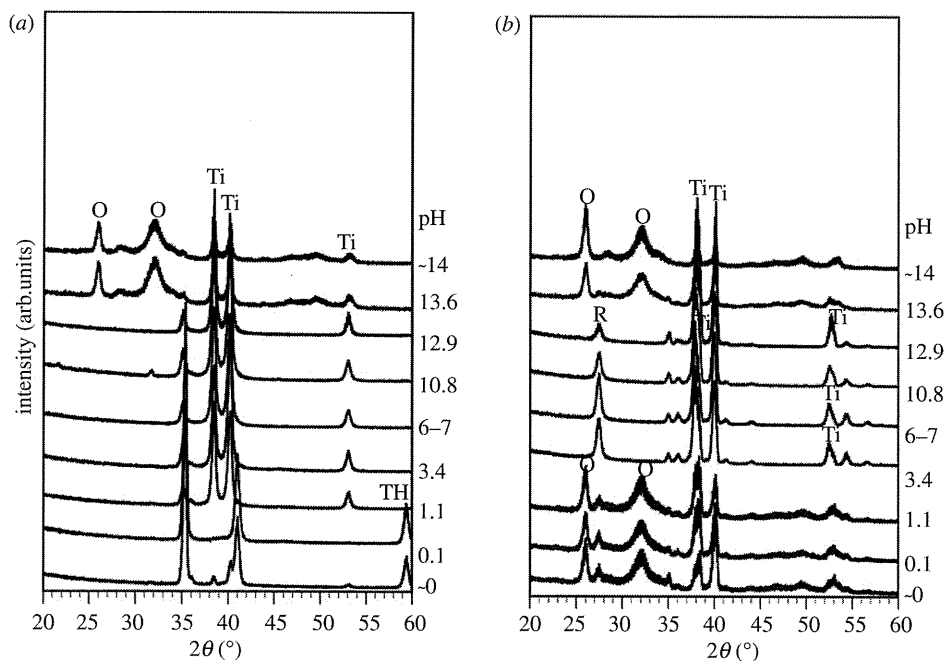


Figure 6. (a) Before and (b) after heat treatment. TF-XRD patterns of surfaces of Ti soaked in SBF for 3 days after exposure to solution with different pHs, and those after subsequent heat treatment, Ti, α Ti; TH, titanium hydride; R, rutile; O, apatite.

exposure to solutions with different pHs, and also those after the subsequent heat treatment. The TF-XRD patterns in figure 6 are of the surfaces of the Ti specimens soaked in SBF for 3 days after exposure to the solutions with the different pHs, and also those after the subsequent heat treatment. The spherical particles observed in the FE-SEM micrographs of the Ti surfaces were identified as crystalline apatite from the XRD

patterns in figure 6. The Ti specimens as exposed to the solutions did not form the apatite on their surfaces except in the case of the solutions with pHs higher than 13.6, where only a relatively small amount of apatite was formed. In contrast, the Ti specimens after the heat treatment exhibited a large amount of apatite on their surfaces when they were exposed to solutions with a pH lower than 1.1 or higher than 13.6.